6 Point Target Detection System for Space Debris

6.1 Introduction

There are many advantages to supplementing ground based radar debris detection systems with optical systems. For example: objects with a low radar signature can still be optically bright (and vice versa); in the field of space debris optical detection is less sensitive to range; the minimum detectable debris size for a given range is less than that for radar. Destructive debris can be as small as one centimetre, so any improvement in detection sensitivity towards this standard is important.

To improve the accuracy of debris orbital elements, a real-time detection system might be preferable in contrast to one in which images are stored for post-observation ("daytime") analysis. This is because more than one telescope is needed to lengthen the observing baseline and so increase the detected fraction of the debris orbit. Therefore, any software based at one telescope that recognises debris in its field of view, produces a first approximation of its orbit elements and alerts extra telescopes along track, must process its data quickly, and preferably during the same pass.
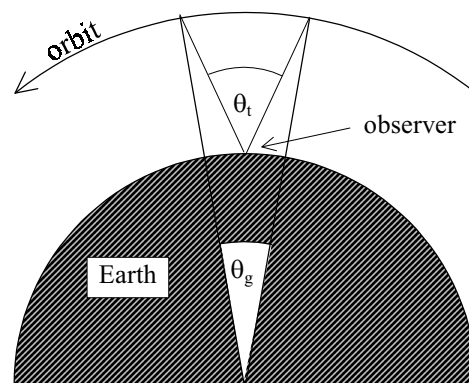

Figure 6.1 Illustration of relationship between topocentric field of view θ_t and true amount of orbit observed arc actually covers (θ_g); see text.

An instantaneous observation from one viewing site cannot provide all of the information about that body's orbit. The geocentric angle subtended by the topocentric field of view comprises only a small fraction of an orbit for a typical field of view of $\sim\frac{1}{2}°$ (see Figure 6.1). With topocentric angular velocities of the

order of those depicted in Figure 6.2, the result is that debris spends only a small amount of time within the field of view for LEO and MEO (Figure 6.3). The curve for tracking ON included in both Figure 6.2 and Figure 6.3 is added for comparison to illustrate the fact that the Earth's rotation imparts an additional 15"s^{-1} to the topocentric angular speed, thus reducing the time in the FOV for all but extremely high orbits above $\approx$60,000 km. The calculations for that curve were made following Lobb and Dick (1992) which state:

$$\omega_{top} = \frac{na}{(a - r_e)} \; , \tag{6.1}$$

where from Kepler's equation,

$$n^2 a^3 = \mu \; , \tag{6.2}$$

where n = geocentric mean motion of the debris (radians s^{-1}), a = semimajor axis of the debris orbit (m), and r_e = radius of Earth (m).

With such a small fraction of the orbit monitored, the orbital eccentricity would be poorly defined. The apparent angular velocity could be used as an indicator for the semimajor axis if the eccentricity is assumed to be zero for example, but with little knowledge of the actual eccentricity the errors induced might propagate after a few orbits to render reacquisition of the particle unlikely. Eccentricity might be gleaned from rate of change of ω_{top} but with a short arc this change would be very small.

The debris should therefore be monitored over as large a fraction of its orbit as practicable to improve the accuracy of the orbital elements. In order to achieve this an ideal optical survey system could be conceived of as comprising a global network of small sites, each containing a telescope in "stare" mode, continually pointing in one altazimuth direction, and a smaller tracking telescope. The stare scope and its attendant camera system and software would make the initial detection of debris in real-time and instruct the on-site tracking scope to make further observations. A basic determination of the debris orbit could be made and this could be used to determine which sites in the network would be further downrange from the first, and experiencing appropriate illumination conditions. If the sites were close enough together, errors caused by assuming zero orbital eccentricity would still be small. Rough positioning information would then be transmitted in real-time to these sites, which could then reacquire the debris and

refine its orbit further. In this way the network would be able to offer a wider baseline of observations during one orbit.
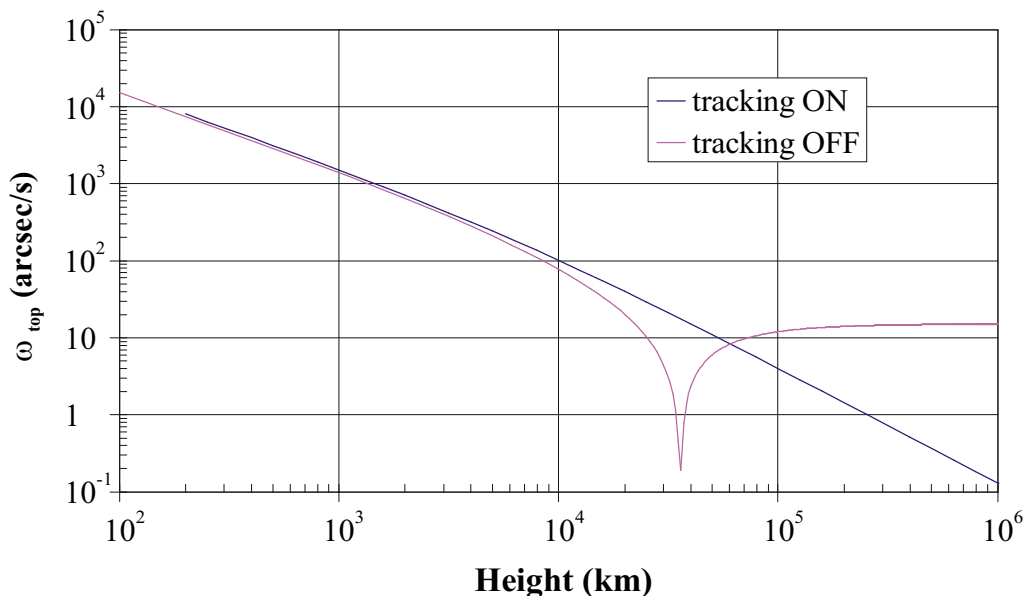

Figure 6.2: Instantaneous topocentric angular velocity at the zenith for a coplanar equatorial system, i.e. one in which the observer and orbit both lie in the plane of the equator, and where sidereal tracking is either on or off. The dip near 40,000 km is due to stationary motion at geostationary height. Dips are non-zero due to sampling frequency of generating code. Asymptote at 15.04"/sec of non-tracking curve is due to near-zero geocentric velocity allowing Earth rotation to dominate.

6.2 Requirements of such a detection system

A debris detection system must be able to meet the following criteria:

- It is desirable for the algorithm to operate quickly without ignoring valid particle tracks. The detection and orbital identification of debris in near real-time allow more timely collision hazard assessments to be made.

- It must also minimise the possibility of false alarms caused by noise in the system. By necessity of being able to detect small debris the system must probe into low signal-to-noise ratios (SNRs) due to their apparent faintness.

These points are discussed in more detail in the following subsections.

6.2.1 Real Time Response through the FOV

The system must be capable of recognising the presence of space debris within its FOV while the debris is passing through it. If it has some downtime for processing, it must know about likely detection rates - could incur some impact on duty cycle. For our purposes we consider only detect-while-in-FOV scenario.
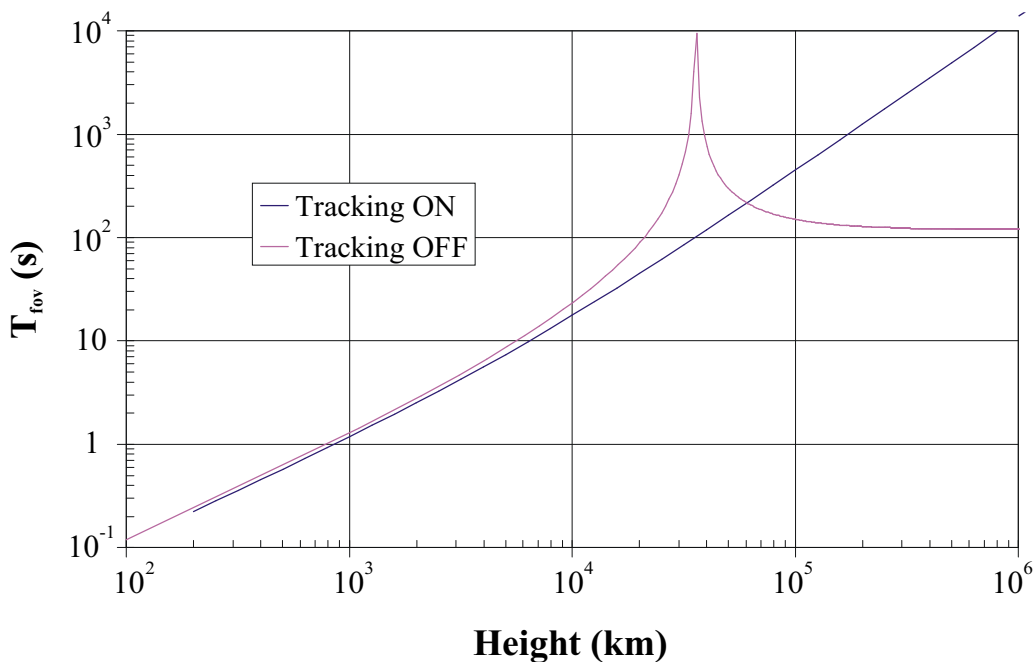
Figure 6.3: Duration of debris visibility in an example ½º-wide field for zenith-pointing equatorial coplanar scenario. Asymptote of non-tracking curve near 40,000 km due to stationary motion around geostationary altitude (finite values caused by sampling frequency of generating code). Asymptote of same curve at $T_{fov} = 119.7s$ due to near-zero geocentric velocity allowing Earth rotation to dominate.

The program has to process the raw images into a form the detection algorithm can understand, then perform the debris detection itself. Any debris detected must have its orbit roughly calculated, and the relevant details written out into a file for analysis later. In the field, such a system would also alert relevant observatories downrange.

All of this "duty cycle" must be accomplished in a timescale that varies according to orbital height. With reference to Figure 6.3, duration within a typical FOV for a typical orbit-observer configuration can be summarised as follows:

Orbit Height	Duration (non-tracking case)	Duration (tracking case)
< 1,000 km	< 1s	less
1,000 – 10,000 km	1s - 1 min	less
> 10,000 km	1 min - hours	~ 2 min

Table 6.1: Summary of timescale for duty cycle.

It can be seen from Table 6.1 and Figure 6.3 that although these figures are only for a simplified 2D case, they give a ballpark estimate of the time available

to the duty cycle, and show that the environment is more forgiving with an increase in orbital height in the case of non-tracking telescope.

Chapter 2 discussed the differences resulting from look angles away from the zenith and non-zero latitude and orbit inclination. The general trend is that angular speed decreases with zenith distance for all cases, and increases with inclination for a given latitude. Implications on duration are therefore that it increases away from the zenith for all orbital heights - an option should the duty cycle be too slow for some low orbits.

6.2.2 Highest Sensitivity Possible - Dwell Time

One of the ways of increasing sensitivity, and therefore the signal-to-noise ratio, is to minimise the exposure (or "integration") time for each CCD frame to be only as long as necessary. Any longer would merely increase the amount of sky noise entering each pixel. To do that one must match the integration time to the "dwell time", this being the amount of time a debris particle image takes to traverse a pixel area in the focal plane of the telescope.

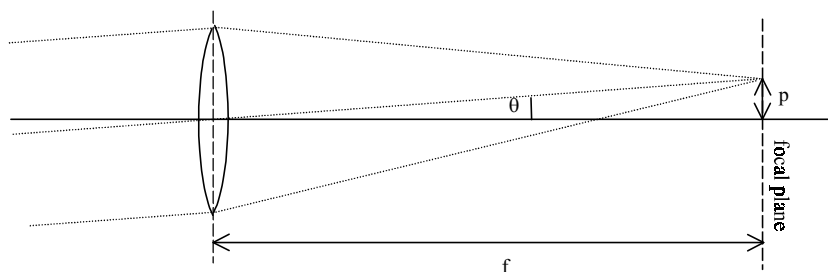The dwell time t_{dw} is clearly therefore a function of the debris' topocentric angular velocity.

Figure 6.4: Illustration of plate scale. Telescope optics can be reduced to a simple objective lens with a focal length f. Setting an offset small angle θ enables one to define the plate scale using simple trigonometry.

With reference to Figure 6.4, a focal length "f" and an offset angle "θ" gives an offset distance "p" at the focal plane, of:

$$p = f \tan \theta , \tag{6.3}$$

where p is the plate scale, usually quoted in micron/arcsec. For a typical 8 inch (20cm) Schmidt-Cassegrain, the focal length is about 2000mm. Hence to determine the plate scale in units of microns per arcsecond, we insert values of $f = 2 \times 10^6$ μm, θ = 1 arcsecond = (1/3600)º, to obtain:

$$p = 2\times10^6 \ \tan (1/3600) \ , \tag{6.4}$$

$$= 9.7 \ \mu\text{m arcsec}^{-1} \ . \tag{6.5}$$

The angular velocity can therefore be expressed in terms of linear focal plane dimensions:

$$v_{top} = \omega_{top} \ p \ . \tag{6.6}$$

The dwell time t_{dw} in one pixel can therefore be found:

$$t_{dw} = \frac{d_p}{v_{top}} \ \ = \frac{d_p}{\omega_{top} \ p} \ , \tag{6.7}$$

where d_p is the path length across the pixel. This can change with orientation across the CCD (Figure 6.5a,b). The maximum possible dwell time occurs when the path follows the diagonal across the pixel. For square pixels the max-min ratio is therefore

$$\left(\frac{t_{dw\,max}}{t_{dw\,min}}\right)_{square} = \sqrt{2} \ , \tag{6.8}$$

(see Figure 6.5a), while for rectangular pixels the ratio depends on the pixel height-width ratio y/x and is given by:

$$\left(\frac{t_{dw\,max}}{t_{dw\,min}}\right)_{rec\,tan\,gular} = \left[1+\left(\frac{y}{x}\right)^2\right]^{\frac{1}{2}} . \tag{6.9}$$
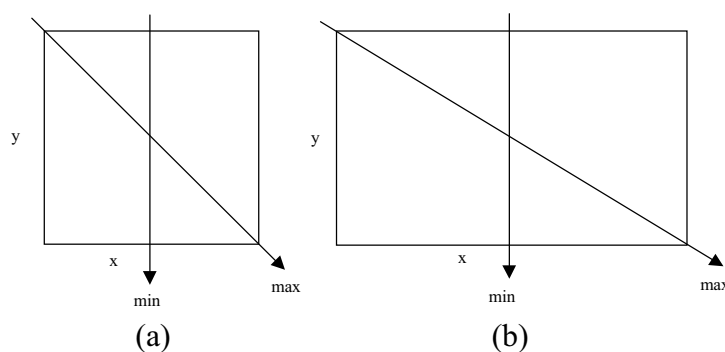

Figure 6.5: Illustrating the difference that path orientation makes with dwell time for (a) square pixels, and (b) rectangular pixels.

6.2.3 Determination of Orbital Characteristics

As test images were taken with the telescope pointing near the zenith and with sidereal tracking on, the equations by Dick (1991) are appropriate and are reproduced here with appropriate change of notation. The orbit is also assumed

to be circular as this makes determination of orbital elements easier and thus increases computing speed. This also introduces inaccuracies if the actual orbit departs appreciably from circular, but this is the best that can be achieved with such a short observation arc. The orbit would be refined by further detections downrange.

Using the following notation:

observed	ω_{st} = siderostatic topocentric angular speed (rad/s)
	θ = angle of trajectory relative to East (North = 90º) (rad)
	τ = local mean sidereal time of observation
known	Φ = longitude of observing site (rad)
	r = geocentric distance of observing site (m)
	μ = Gravitational constant for the Earth (3.987×10^{14} N m^2)
to calculate	a = semimajor axis (m)
	n = mean motion (rad/s)
	i = orbit inclination (rad)
	κ = orbital longitude of debris measured from Ω (rad)
	Ω = longitude of ascending node (rad)
	h = height at zenith (a - r) (m)

the equations

$$\omega_{st} = \frac{na}{(r-a)} \tag{6.10}$$

and
$$n^2 \, a^3 = \mu \tag{6.11}$$

are combined to form a cubic in $\sqrt{a}$,

$$a^{\frac{3}{2}} - ra^{\frac{1}{2}} - \frac{\mu^{\frac{1}{2}}}{\omega_{st}} = 0 \ , \tag{6.12}$$

which is computationally more efficient to solve numerically using an iterative procedure (Newton-Raphson).

The inclination is given by:

$$i = \cos^{-1}(\cos \Phi \cos \theta), \tag{6.13}$$

while the longitude of the ascending node is calculated from:

$$\Omega = \tau - \tan^{-1}\left[\frac{\sin \Phi}{\tan \theta}\right]. \tag{6.14}$$

6.2.3.1 Effects of Errors on Downrange Predictions

After an initial detection, the observables ω_{top} and θ would be used to predict the position of the debris particle after a time t, corresponding to a downrange angle of α, i.e. the great circle arc produced by the movement of the debris during the time t.

Errors in the initial determination of ω_{top} and θ increase with α however[*], resulting in an offset of the debris' true position from its predicted position at any time. This would therefore cause a corresponding offset from the zenith, Δz, for an observer directly below the predicted position. Following Dick (1991), the resulting offset can be resolved into orthogonal along-track (Δz_i) and cross-track (Δz_j) components. Figure 6.6 and Figure 6.7 illustrate the derivation of these components separately.
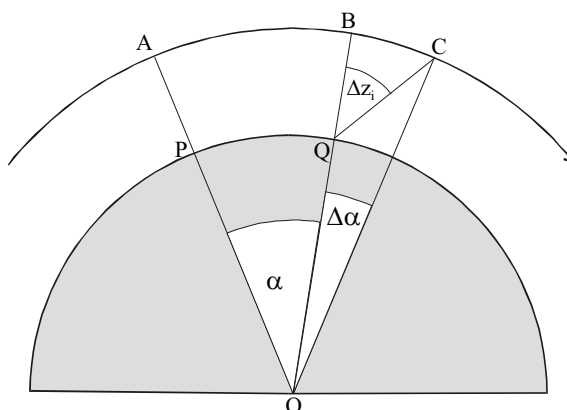

Figure 6.6: Construction for along-track errors. An error in initial determination of ω_{st} at A by an observer at P causes prediction of debris to be at B after a downrange angle α when it is actually offset by an angle $\Delta\alpha$ at C. An observer at Q would observe the debris at a zenith distance Δz_i.
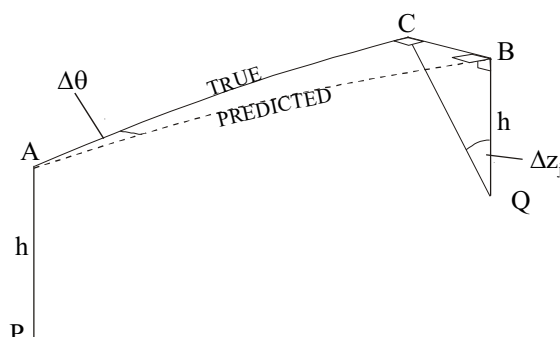

Figure 6.7: Using similar notation as in Figure 6.6, an error $\Delta\theta$ in orbit direction causes an offset perpendicular to the direction of motion, viewed as an offset zenith distance of magnitude Δz_j.

---

[*] Along-track errors would propagate continuously, whereas across-track errors reach a maximum effect at 90º and 270º from the initial point.

After a track length angle α and assuming small angles, the components can be given by:

$$\Delta z_i = \Delta \omega_{st} \alpha \left(\frac{a^3}{\mu} \right)^{\frac{1}{2}} , \qquad (6.15)$$

and
$$\Delta z_j = \frac{a}{h} \cos^{-1}\left[\cos^2 \alpha + \sin^2 \alpha \cos(\Delta \theta) \right] . \qquad (6.16)$$

The magnitude of the offset is therefore given by (assuming small angles):

$$\Delta z = \sqrt{\Delta z_i^2 + \Delta z_j^2} . \qquad (6.17)$$

Given this information, the accuracy requirements of a debris trail in the FOV of a second tracking telescope may be calculated if one considers a requirement to be that the debris must be within the FOV at the predicted time, if the FOV is centred on the predicted coordinates. With a typical FOV to be ~ 0.5°, if one assumes the allowable position error at the zenith to be 0.25° (topocentric), then from equations (6.15), (6.16) and (6.17) the following tolerances for ω_{top} and θ_{top} are given by Figure 6.8 & Figure 6.9 respectively.
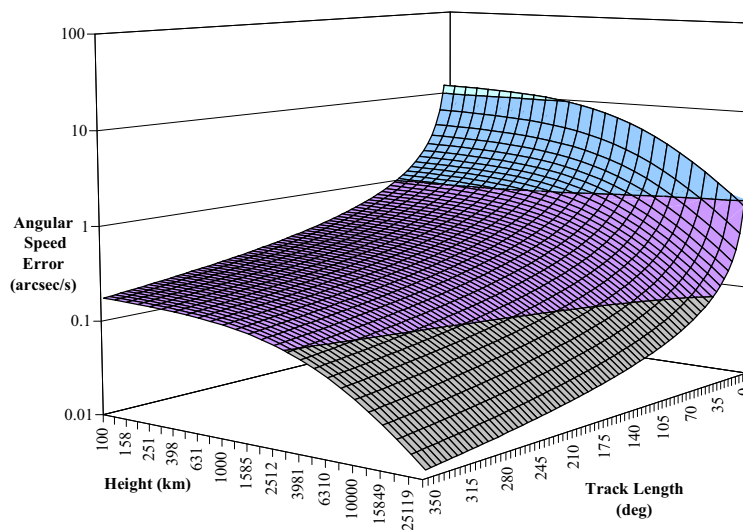

Figure 6.8: Tolerance of ω_{top} to putting a debris particle within 0.25° of the centre of FOV of a second telescope an angular distance (track length) downrange.
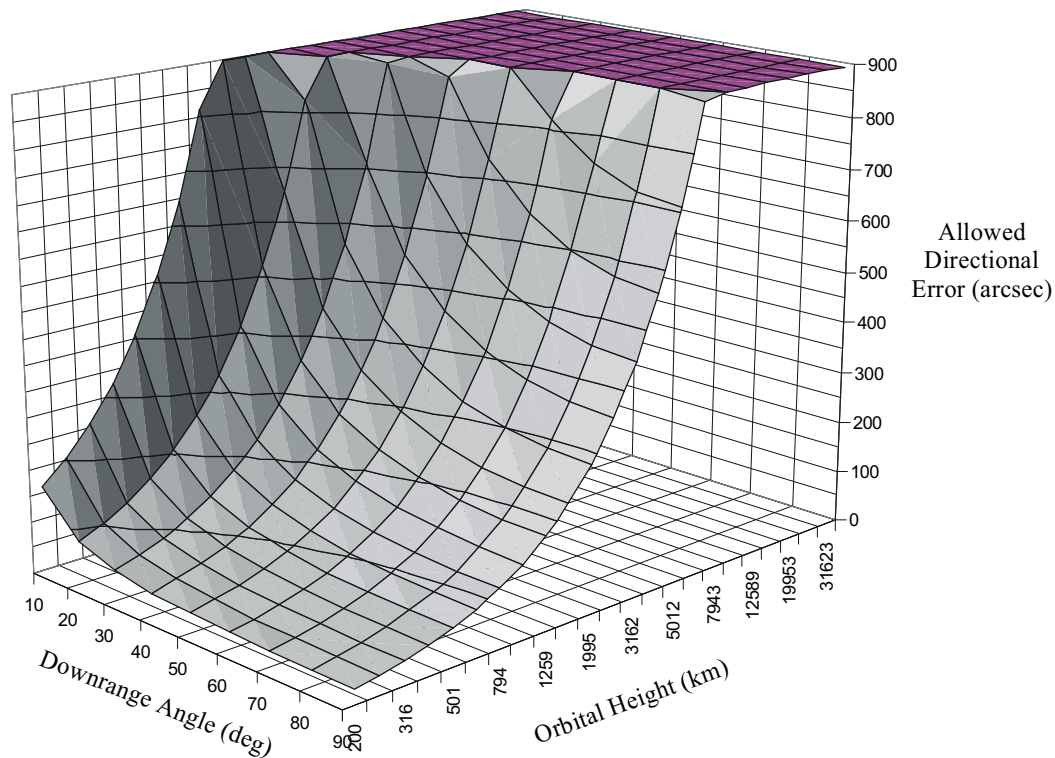
Figure 6.9: Accuracy requirements for determining the direction of the topocentric angular motion of debris to ensure its positioning within 0.25º of a secondary telescope downrange. The graph is truncated for values above 900 arcsec.

6.3 Herstmonceux Camera System

The main driver behind the structure of the debris detection algorithm specified in the next chapter was that it had to process data from the camera system used at the Satellite Laser Ranger (SLR) of the Royal Greenwich Observatory (RGO) at Herstmonceux.

Circumstances led to the cessation of collaboration with the RGO on this matter, by which time the basic structure of the program had been frozen. The program can be used with CCD imagery from any telescope system however, provided some processing is done to mimic that which the RGO camera was configured to do; details of which may be found in chapter 8.

The following subsections describe the RGO camera's processes to illustrate the design drivers for the main structure of the program featured in the next chapter.

6.3.1 Herstmonceux camera system "front end"

The following subsections describe first the layout of the telescope, camera, and processing system at the SLR.
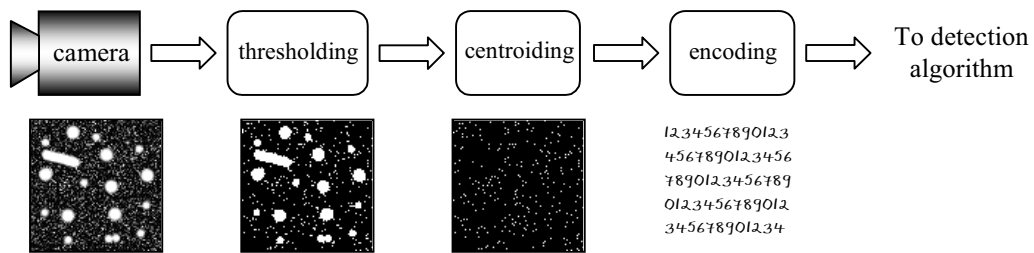
Figure 6.10: Block diagram of the "front end" of the camera system at Herstmonceux showing the stages of preanalysis image processing that takes place, with illustrative pictures underneath each step.

6.3.1.1 Telescope

The "front end" of the system that the DDT package was initially designed for consists of a Celestron 20cm (8 inch) Schmidt Cassegrain telescope (SCT) mounted piggyback on the main telescope at the SLR. The main telescope itself is a computer-controlled Schmidt on an altazimuth mount.

6.3.1.2 Camera

Mounted on the SCT is a Princeton Instruments Inc. Peltier-cooled CCD camera operated in conjunction with a custom image processing package written in-house.

6.3.1.3 Computing equipment available

Raw frame data from the camera is fed to the processing package where it is thresholded and centroided using an intensity weighted "centre of gravity" technique. The centroids are then run-length encoded and the resulting sorted list of centroids is fed to the post-processing computer.

6.3.2 Image processing details

Pre-processing of the incoming CCD frames, prior to analysis by the DDT program is discussed here in detail.

6.3.2.1 Thresholding

The raw frame is an 8-bit graylevel image. Thresholding converts this into a binary image containing just two graylevel values. Each pixel is compared to a threshold level, set between 0 and 255 (for an 8-bit image), and if it falls below this value, its value is set to 0. If above the threshold, its value is set to 1.

The thresholding algorithm is common to any image processing software and can be written in the form:

$$g(x,y) = \begin{cases} G_{255} & \text{if } f(x,y) > T \\ G_0 & \text{if } f(x,y) \leq T \end{cases}, \qquad (6.18)$$

where g(x,y) is the thresholded image, f(x,y) is the original image, and $G_{255,0}$ are the graylevels assigned to the pixel if above or below the threshold level T, respectively.

6.3.2.2 Centroiding

Centroiding is the act of finding the geometric centre of an object in the image. Centroiding is performed because it is computationally easier to deal with a single point to represent an object. The algorithm used is given by (from Myler and Weeks, 1993):

$$X_c = \frac{1}{A} \sum_{i=1}^{N} X_i, \qquad Y_c = \frac{1}{A} \sum_{i=1}^{N} Y_i.\qquad (6.19)$$

Here X_i, Y_i are the coordinates of pixel i in the object, A is the object area in units of pixels, and X_c, Y_c are the centroid coordinates.

6.3.2.3 Run Length Encoding

Run length encoding (RLE) is a compression algorithm that is good for images containing lots of the same colour. It takes a repeat count of homogenous areas of the image, rather than assign values to each pixel. For an image of the sort output by the camera, this routine is useful as there are large number of images taken in just one night.

6.3.2.4 Resulting system restrictions

Faced with this data format, any possible initial recognition of debris from the image itself would be impossible. Stars, debris, and any noise that survived the thresholding process would all look alike - no information about the origin of the centroids is kept; effectively the processed imagery is just a list of positions of centroids (referred to hereafter as "dots").

6.4 Summary

Basic requirements for a real-time detection system in terms of speed and accuracy were presented. The system was shown to be required to perform analysis in under a second for LEO, tens of seconds up to MEO, and in minutes

to hours for high Earth orbit. The dwell time t_{dw} was introduced as a measure of the time taken for the debris image to traverse one pixel, and was shown to be the optimum integration time for debris detection. Slight adjustments to the dwell time to incorporate rectangular pixels were discussed.

Basic equations for the determination of orbital elements assuming circular orbits were presented, along with a quantitative discussion of the effects of errors on speed and direction of the detected debris track at the first telescope on placement of the debris within the FOV of a second telescope downrange.

The main design driver for the design of the debris detection program presented in the next chapter was presented as the camera system in use at the Satellite Laser Ranger at the RGO site at Herstmonceux. Processing performed by the camera system was described and the state of its output described, also in terms of restrictions to subsequent analysis by the detection algorithm.